**Showcasing research from Professor HANAOKA's laboratory, Graduate School of Pharmaceutical Sciences, Keio University, Tokyo, Japan.**

Development of a silicon phthalocyanine analogue for near-infrared photoimmunotherapy and its application to HTLV-1-infected leukemic cells

Near-infrared photoimmunotherapy (NIR-PIT) employing an antibody labelled with a silicon phthalocyanine dye, IR700, was approved in 2020. However, further derivatization of IR700 is needed to increase the efficiency of cancer treatment. We newly developed SiPc-1 as an IR700 analog, in which the linker was constructed using click chemistry to simplify the synthetic scheme and its position was switched from α to β on the benzene ring of phthalocyanine to eliminate intramolecular steric repulsion. An anti-CD25 antibody, basiliximab, labelled with SiPc-1 showed selective toxicity towards human T-cell lymphotropic virus type 1 (HTLV-1)-infected cells.

Image reproduced by permission of Kenjiro Hanaoka from *RSC Chem. Biol.*, 2025, **6**, 1576.
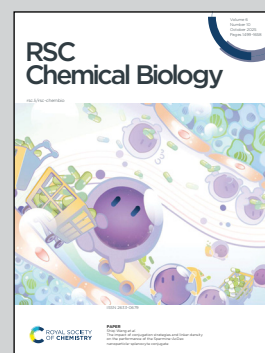
ROYAL SOCIETY OF CHEMISTRY

rsc.li/rsc-chembio

Check for updates

Development of a silicon phthalocyanine analogue for near-infrared photoimmunotherapy and its application to HTLV-1-infected leukemic cells

Yoshikazu Fuse, [iD][a] Eita Sasaki, [iD][a] Masaharu Tamaki,[cd] Shunto Kawamura,[cd] Hisashi Ohno, [iD][a] Sota Yamada, [iD][a] Masahiro Yasunaga,[e] Hideo Takakura, [iD][f] Hirofumi Hanaoka, [iD][f] Hisataka Kobayashi,[fg] Hideki Nakasone [iD][cd] and Kenjiro Hanaoka [iD]*[ab]

Near-infrared photoimmunotherapy (NIR-PIT) employing an antibody labeled with a silicon phthalocyanine dye, IR700, was approved as a minimally invasive treatment for unresectable recurrent head and neck cancer in Japan in 2020. However, further derivatization of IR700 is needed to increase the efficiency of cancer treatment. Here, we developed **SiPc-1** as an IR700 analog, in which the linker was constructed using click chemistry to simplify the synthetic scheme and its position was switched from α to β on the benzene ring of phthalocyanine to eliminate intramolecular steric repulsion. We evaluated the cleavage rate of the water-soluble axial moieties of **SiPc-1** upon photoirradiation, the cytotoxicity, and the morphological change (blebbing) of treated cells upon photoirradiation. We performed gene expression and protein expression analyses to find a target antigen selectively expressed on cells infected with human T-cell lymphotropic virus type 1 (HTLV-1), the causative virus of adult T-cell leukemia/lymphoma (ATL), and identified CD25 as a suitable target antigen. An anti-CD25 antibody, basiliximab, labeled with **SiPc-1** (bas-**SiPc-1**) showed selective toxicity towards HTLV-1-infected cultured cells and ATL patients' peripheral blood mononuclear cells upon photoirradiation.

Introduction

Near-infrared (NIR) light shows high tissue penetration and causes minimal tissue damage. To take advantage of these features, NIR light has been employed in photodynamic therapy (PDT) for cancer treatment, using photosensitizers that generate singlet oxygen in response to NIR light irradiation,[1] thereby inducing the necrosis of cancer cells.[2,3] However, since the photosensitizers do not have high tumor-targeting ability, normal cells surrounding tumor cells may also be damaged. To overcome this issue, near-infrared photoimmunotherapy (NIR-PIT) has been developed to induce NIR light-dependent cell death in target tumor cells by using conjugates of monoclonal antibodies with the photosensitizer IR700 (Ab-IR700).[4,5] Cancer targeting is achieved by utilizing antibodies targeting antigens that are selectively expressed on cancer cells. These antibodies direct the conjugates to the target cells, and consequently activation of IR700 upon NIR photoirradiation selectively kills tumor cells in the irradiated areas, affording a therapeutic effect.[4,5]

In NIR-PIT, the photoirradiation cleaves the hydrophilic moieties of the dye, transforming its character from hydrophilic to hydrophobic.[4] This results in membrane damage of the target cells, probably due to the aggregation of Ab-IR700 and the target antigen, leading to cell death.[4] Moreover, after NIR-PIT treatment, the release of damage-associated molecular patterns (DAMPs) activates antitumor immunity, providing secondary therapeutic effects.[6] In 2020, the NIR-PIT drug, Akalux®[7,8] was approved for unresectable locally advanced or locally recurrent head and neck cancer in Japan. Furthermore, clinical trials on esophageal and uterine cervical cancers are currently underway, and this therapeutic approach may also be extended to other types of cancers.

[a] *Graduate School of Pharmaceutical Sciences, Keio University, 1-5-30, Shibakoen, Minato-ku, Tokyo 105-8512, Japan. E-mail: khanaoka@keio.jp*

[b] *Human Biology-Microbiome-Quantum Research Center (WPI-Bio2Q), Keio University, Tokyo 108-8345, Japan*

[c] *Division of Hematology, Jichi Medical University Saitama Medical Center 1-847, Amanuma-cho, Ohmiya-ku, Saitama 330-8503, Japan*

[d] *Division of Emerging Medicine for Integrated Therapeutics (EMIT), Center for Molecular Medicine, Jichi Medical University, Shimotsuke, 329-0498, Japan*

[e] *Division of Developmental Therapeutics, Exploratory Oncology Research and Clinical Trial Center, National Cancer Center, Chiba 277-8577, Japan*

[f] *Near InfraRed Photo-ImmunoTherapy Research Institute, Kansai Medical University, 2-5-1 Shin-machi, Hirakata, Osaka 573-1010, Japan*

[g] *Molecular Imaging Program, Center for Cancer Research, National Cancer Institute, National Institutes of Health, Bethesda, Maryland 20892-1088, USA*

a)

b) c)
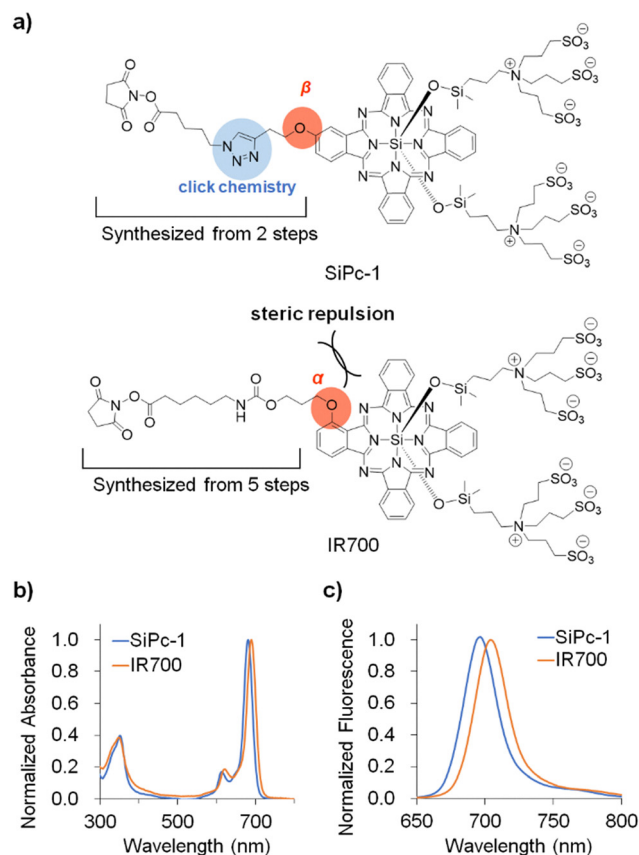
Fig. 1 (a) Comparison of the structures of **SiPc-1** and IR700. (b) Absorbance spectra of **SiPc-1** (1 μM) and IR700 (1 μM) in Dulbecco's phosphate-buffered saline (DPBS) (pH 7.4). (c) Fluorescence spectra of **SiPc-1** (1 μM) and IR700 (1 μM) in DPBS (pH 7.4).

However, NIR-PIT still has some limitations. For example, the penetration depth of NIR light in tissues is limited to a few centimeters, making its application to deep-seated tumors or large tumor masses difficult. Moreover, some patients experience transient acute edema after the treatment,[9,10] which may be due to the release of reactive oxygen species (ROS) from IR700 upon NIR light irradiation.[11,12] Therefore, there is a need for photosensitizers that have a longer absorption wavelength than IR700 and can be activated with lower doses of NIR light. In this study, we designed a IR700 analogue, **SiPc-1**, to meet these requirements, and developed a shorter synthetic route compared to the scheme employed for IR700. Our results suggest that **SiPc-1** and related IR700 analogues may be promising candidates as photosensitizers for improving the therapeutic efficacy of NIR-PIT.

Results and discussion

Design and synthesis of SiPc-1

In designing the synthetic scheme for IR700, we focused on the following two points. (i) Steric repulsion impedes the synthesis of the phthalocyanine skeleton from a linker-substituted monomer and three unsubstituted monomers (Fig. 1a), probably

because the unsubstituted monomers react with each other preferentially, making it difficult to produce the 1+3-type phthalocyanine containing a linker-substituted monomer. To overcome this problem, we changed the location of linker substitution from the α-position to the β-position of the phthalocyanine backbone. (ii) In the synthesis of IR700, elongation of the linker moiety is performed after the water-soluble axial moieties are conjugated to the silicon phthalocyanine skeleton. However, this involves four steps. Thus, we aimed to reduce the number of steps by utilizing click chemistry, *i.e.*, Huisgen 1,3-dipolar cycloaddition, to synthesize the linker moiety. We therefore designed the synthetic procedure shown in Scheme 1 for the synthesis of **SiPc-1**.

To obtain **SiPc-1**, we firstly synthesized the linker-substituted monomer **2** in two steps, whereas five steps are needed for the synthesis of the linker-substituted monomer in the synthetic scheme for IR700. The linker-substituted monomer for IR700 is protected by PMB (*p*-methoxybenzyl) group, which has to be deprotected for the linker elongation in a later step. However, **2** has an alkyne group, which does not require a deprotection step for the linker elongation. Compound **2** reacted with the non-substituted monomer (1,3-diiminoisoindoline) in a 1:2 molar ratio, affording **3** as a mixture. Next, **6** was synthesized from **3** in three steps using a similar method to that employed for IR700.[13]

Compound **7** was obtained by Huisgen 1,3-dipolar cycloaddition[14] with **6** and Sodium 5-azidovalerate. Finally, NHS esterification of **7** was performed to obtain **SiPc-1** (8 steps, total yield: 0.6%), which is an amino-reactive form.

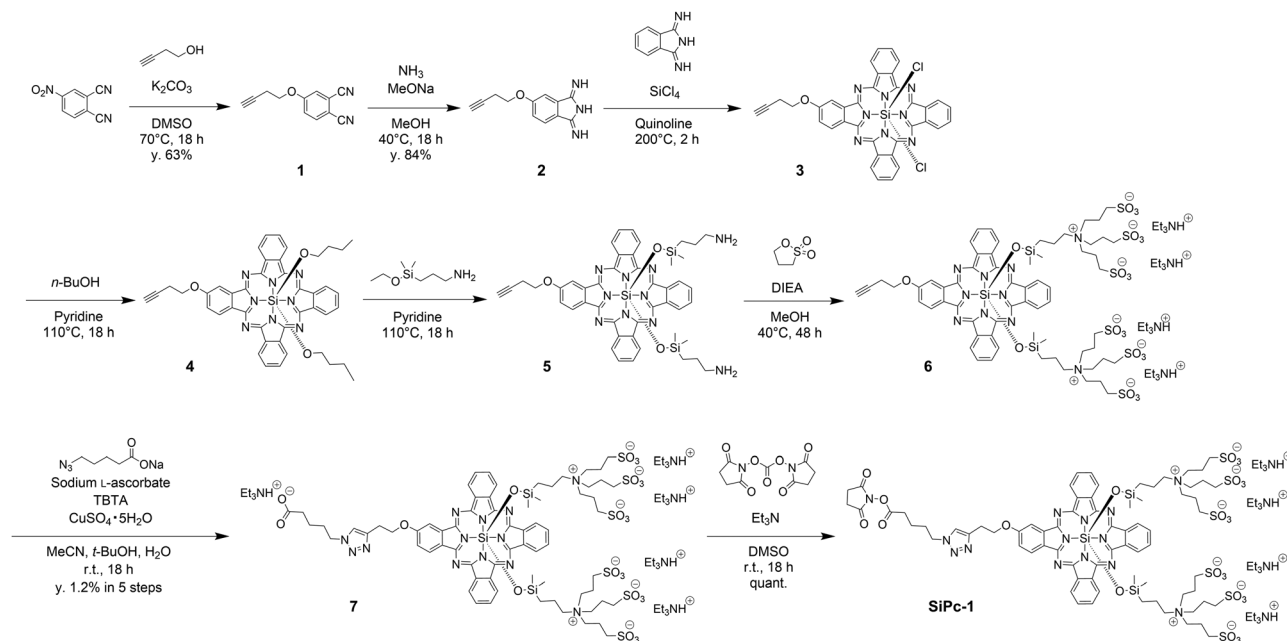### Assessment of photophysical properties

We first examined the absorption and fluorescence spectra of **SiPc-1**. Compared to IR700, the wavelengths of maximum absorbance and fluorescence of **SiPc-1** were blue-shifted by 9 nm and 10 nm, respectively (Table 1 and Fig. 1b, c). The fluorescence quantum yields were 0.29 for **SiPc-1** and 0.26 for IR700 (Table 1). Thus, **SiPc-1** has very similar photophysical properties to IR700. Further, the $\log P_{o/w}$ of **SiPc-1** was −0.48, which indicates that **SiPc-1** is very hydrophilic. Furthermore, the absorption spectra of **7** in DPBS (pH 7.4) with or without 4% w/v human serum albumin (HSA) were measured and the spectral change was not observed, suggesting that **SiPc-1** does not interact with HSA in aqueous solutions (Fig. S1).

Next, we examined whether **SiPc-1** undergoes a photochemical reaction in which the water-soluble axial moieties are cleaved (Fig. 2a), followed by aggregate formation, upon photoirradiation with NIR light (690 nm) in the presence of electron donors, cysteines. It has been shown that loss of the axial moieties changes the character of IR700 from hydrophilic to hydrophobic, and this photochemical reaction is the key to NIR-PIT.[4,15–18]

Loss of the water-soluble axial moieties was confirmed by HPLC analysis of an NIR-photoirradiated solution of **SiPc-1** (Fig. 2b) and the formation of aggregates after the photochemical reaction could be seen with the naked eye (Fig. 2c). We further examined the efficiency of this photochemical reaction compared with that of IR700. The absorption and fluorescence intensity of the **SiPc-1** solution both decreased dependently

© 2025 The Author(s). Published by the Royal Society of Chemistry

RSC Chem. Biol., 2025, **6**, 1576–1584 | **1577**

Scheme 1 Synthesis of **SiPc-1**.

upon the irradiated light dose, in essentially the same manner as those of IR700 (Fig. 2d, e and Fig. S2). These results confirm that **SiPc-1** exhibits IR700-like photosensitivity. On the other hand, in the absence of cysteine, the decrease of absorption and fluorescence intensity of **SiPc-1** under the light irradiation was slight (Fig. S3). This result suggested that the electron donors such as cysteine are necessary to cleave the axial ligands of **SiPc-1** same as IR700.[4] Further, the stability of **SiPc-1** in aqueous solutions with 5 mM cysteine or 5 mM reduced glutathione (GSH) was examined. As a result, **SiPc-1** was stable in aqueous solutions without the light irradiation at least for 3 h (Fig. S4).

Application of SiPc-1 to cultured cells

We then examined whether **SiPc-1** is suitable for NIR-PIT. As models, we employed EGFR (epidermal growth factor receptor)-overexpressing A431 cells derived from a human epithelial carcinoma, and DiFi cells, a human colorectal cancer cell line with a Braf mutation, obtained as previously reported.[19]

First, we prepared an anti-EGFR antibody, cetuximab, labeled with **SiPc-1** (cet-**SiPc-1**) at a drug-to-antibody ratio (DAR) of 2.7 (Fig. S5a and b). We then assessed the specificity of cet-**SiPc-1** for EGFR. Cells treated with cet-**SiPc-1** exhibited strong fluorescence derived from the phthalocyanine structure of **SiPc-1**. Pre-treatment with an excess amount of cetuximab

quenched this fluorescence, indicating that cet-**SiPc-1** retains the antigen specificity of the antibody (Fig. S6).

We next examined the cytotoxicity of cet-**SiPc-1** towards A431 and DiFi cells upon NIR photoirradiation delivered by a full-plate LED-type NIR light irradiation device (670–710 nm emission, Ebisu Electronics Co., Ltd., Japan) (Fig. S7). Although neither cetuximab nor **SiPc-1** alone showed any cytotoxicity, cet-**SiPc-1** showed clear cytotoxicity to both A431 and DiFi cells (Fig. 3a and Fig. S8a). The cytotoxicity increased in a light dose-dependent manner (Fig. 3b and Fig. S8b).

We also observed the morphological change of A431 and DiFi cells treated with cet-**SiPc-1** by fluorescence microscopy. Upon photoirradiation at 640 nm, the cells treated with cet-**SiPc-1** showed the formation of "blebs" similar to those observed with cet-IR700 (Fig. 3c and Fig. S8c). Bleb formation is a shape change characteristically seen in NIR-PIT.[4,5] Moreover, to evaluate whether the cell membrane is damaged after bleb formation, the cells were loaded with a live-cell-staining fluorescent dye, Calcein-AM, which diffuses cytosolically inside the cells, and were irradiated at 640 nm after treatment with cet-**SiPc-1**. As a result, the fluorescence of Calcein disappeared following bleb formation, indicating that the cell membrane was compromised, allowing Calcein to leak out from the cells. These results demonstrate that antibodies conjugated with **SiPc-1** can induce bleb formation on the cell membrane, leading to membrane damage, similarly to IR700. Thus, **SiPc-1** is a promising candidate as a photosensitizing dye for NIR-PIT. Furthermore, A431 and DiFi cells treated with cet-**SiPc-1** in the absence of Calcein dyes were also observed by confocal laser microscopy. Although their morphology was normal before the NIR light irradiation, the fluorescence of **SiPc-1** decreased upon light irradiation, and bleb formation similar to that shown in Fig. 3c and Fig. S8c was observed (Fig. S9). This result suggests that the bleb formation in

Table 1 Photophysical properties of **SiPc-1** and IR700 in PBS (pH 7.4)

	ε (mol^{-1} cm^{-1})	λ_{abs} (nm)	λ_{flu} (nm)	$\Phi_{fl}{}^a$	$\Phi_{\Delta}{}^b$
SiPc-1	224 000	681	694	0.29	0.11
IR700	201 000	690	704	0.26	0.12

[a] Absolute fluorescence quantum yield. [b] Singlet oxygen production quantum yield.
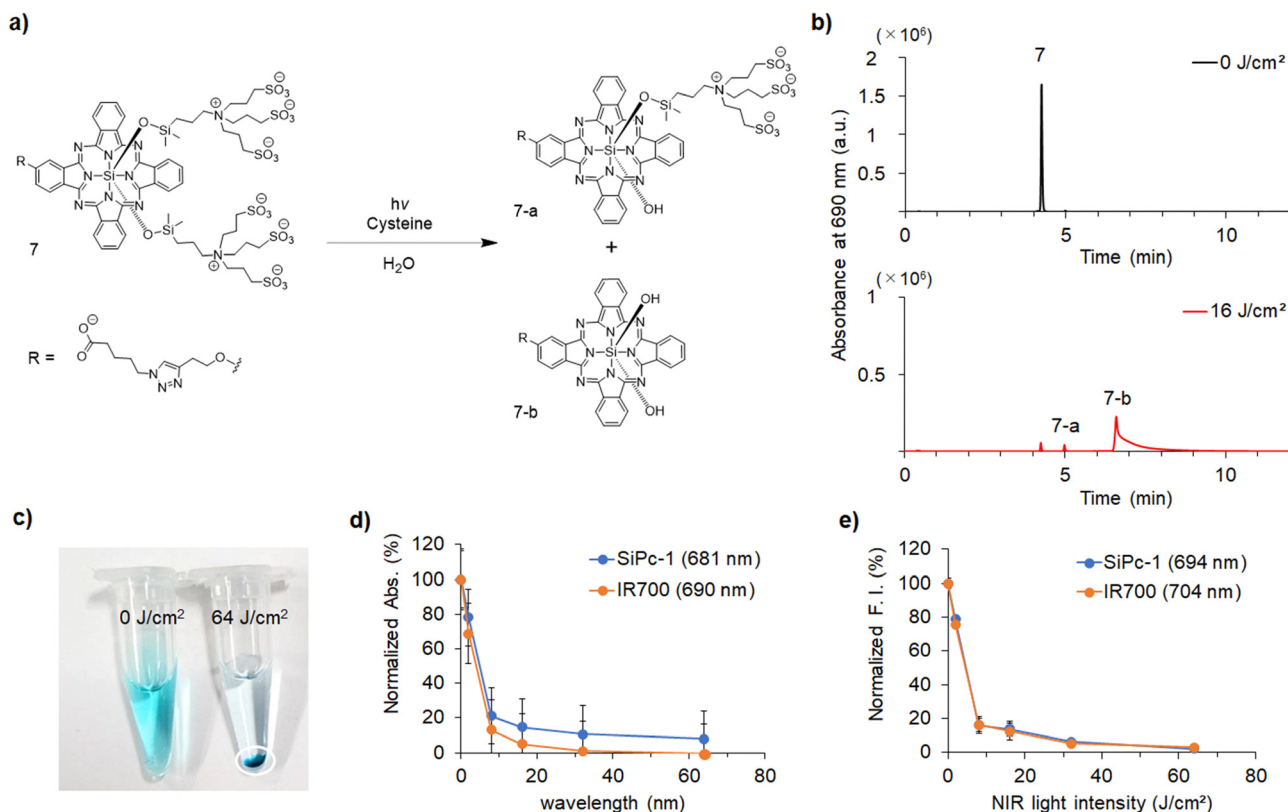
Fig. 2 (a) Photochemical reaction resulting in cleavage of the axial moieties of **SiPc-1**. (b) HPLC analysis of DPBS (pH 7.4) solution containing compound **7** (5 μM) and L-cysteine (5 mM) with (red) or without (black) NIR light irradiation (16 J cm^{-2}) at 690 nm. (c) Aggregation of **SiPc-1** was apparent to the naked eye in the **SiPc-1** solution (20 μM) in DPBS after the NIR light irradiation (64 J cm^{-2}) at 690 nm. (d) and (e) Absorbance (d) and fluorescence intensity (e) of **SiPc-1** and IR700 were measured after NIR irradiation at various light doses (n = 3, error bar: SD).

this experiment is not caused by Calcein, but by the activation of cet-**SiPc-1** upon NIR light irradiation.

Comparison of cytotoxicity between SiPc-1 and IR700

Next, we compared the cytotoxicity of cetuximab conjugated with IR700 and with **SiPc-1**. Cetuximab was labeled with average of 2.7 molecules of IR700 or **SiPc-1** (cet-IR700 or cet-**SiPc-1**). After treatment of A431 or DiFi cells with these conjugates, the cells were washed and irradiated with NIR light. The cytotoxicity of both conjugates was comparable at the irradiation dose of 2 J cm^{-2} or higher. However, at lower doses (0.5, 1 J cm^{-2}), cet-**SiPc-1** exhibited slightly lower cytotoxicity than cet-IR700 (Fig. 3b and Fig. S8b). This difference could be due to easier cleavage of the axial moieties or to higher singlet oxygen production of IR700, compared to **SiPc-1**. However, the singlet oxygen production quantum yield of **SiPc-1** under light irradiation at 690 nm was determined to be 0.11, while that of IR700 was 0.12, indicating that **SiPc-1** produces singlet oxygen at a similar level to IR700 (Table 1). This suggests that the difference in cytotoxicity between **SiPc-1** and IR700 is not due to a difference in the efficacy of singlet oxygen production.

We also examined the cytotoxicity in the presence of 20 mM sodium azide, a singlet oxygen quencher. The results indicated that cet-**SiPc-1** showed almost the same cytotoxicity as cet-IR700 (Fig. 4 and Fig. S10). This indicates that the lower cytotoxicity of
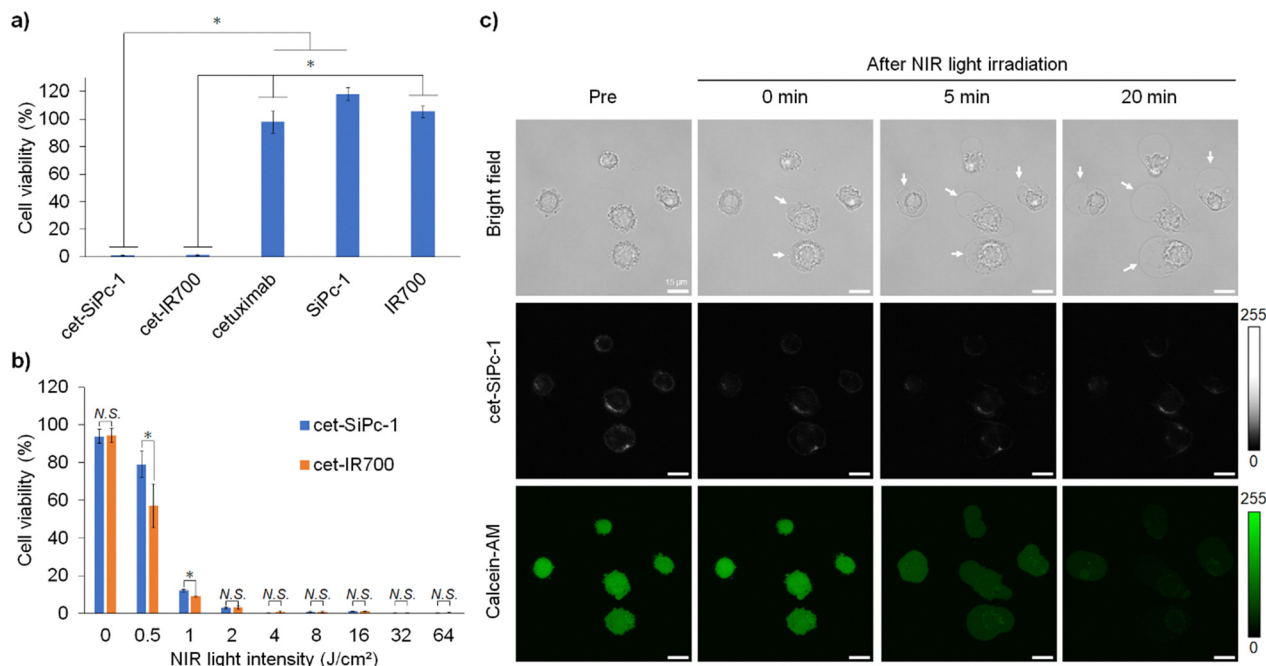
SiPc-1 compared to IR700 may be due to lower aggregation capability after photoirradiation. **SiPc-1** contains a triazole group, which likely inhibits the π–π stacking and the hydrophobic interaction between phthalocyanine rings, and these interactions may be important for aggregate formation, which induces the cell-membrane damage during NIR-PIT. It should be noted that the wavelength of the irradiation light in this experiment (690 nm) corresponds to the absorption maximum of IR700 but not **SiPc-1** (681 nm) and this may also contribute to the cytotoxicity difference between **SiPc-1** and IR700.

Application to ATL

We next investigated whether **SiPc-1** might be available to treat adult T-cell leukemia/lymphoma (ATL). ATL is a hematological malignancy caused by long-term infection with human T-cell leukemia virus type I (HTLV-1)[20–23] and features CD4-positive T cells. Existing treatment options include combination chemotherapy and allogeneic hematopoietic stem cell transplantation (Allo-HCT).[24,25] However, the therapeutic effect of the multidrug combination chemotherapy is limited by the development of drug resistance and there is a high relapse rate.

Furthermore, ATL patients are generally old, and Allo-HCT is contraindicated for many older patients.[26–28] Therefore, the development of novel therapeutic strategies is required. We expected that NIR-PIT with **SiPc-1** would contribute to the

© 2025 The Author(s). Published by the Royal Society of Chemistry

RSC Chem. Biol., 2025, **6**, 1576–1584 | **1579**

Fig. 3 (a) Assay of cytotoxicity against A431 cells ($n = 4$, error bar: SD, $*p < 0.01$). (b) The light-dose-dependent cytotoxicity of cet-**SiPc-1** and cet-IR700 towards A431 cells ($n = 4$, error bar: SD, $*p < 0.01$). (c) Blebs were formed after photoirradiation (640 nm) of A431 cells treated with 10 µg mL^{-1} of cet-**SiPc-1**. Fluorescence images of **SiPc-1** and Calcein are also shown. The fluorescence of Calcein disappeared after the photoirradiation, probably because of cell-membrane damage following the cell blebbing (indicated by arrows). cet-**SiPc-1** channel (Ex. 640 nm, Em. 650–750 nm); Calcein AM channel (Ex. 488 nm, Em. 500–540 nm).

treatment of ATL in terms of greater safety and specificity. We first searched for target antigens that are selectively expressed on HTLV-1-infected cells, in order to select suitable antibodies to be used in NIR-PIT for the treatment of ATL. Gene expression analysis by RNA-seq was performed on HTLV-1-infected cell lines (MT-1, MT-2, MT-4 and ATN-1) and non-infected control T-cell lines (MOLT-4 and TALL-1) (Fig. 5a). As a result, CD25 (IL2RA), IL21R and CCR7 were identified as cell-surface antigens selectively expressed in HTLV-1-infected cells.
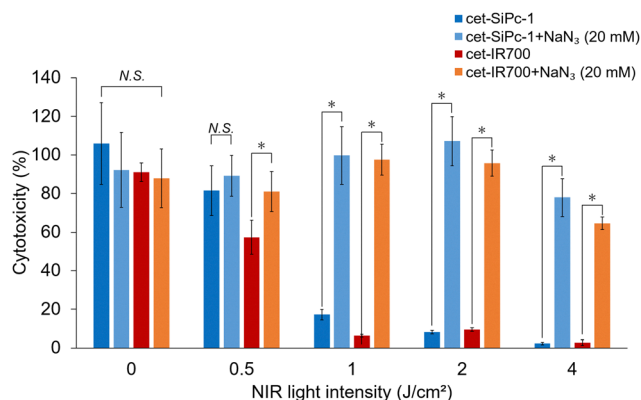
We also examined the protein expression of these antigen candidates in HTLV-1-infected cells (MT-1, MT-2, MT-4, and

Fig. 4 Comparison of the cytotoxicity of cet-**SiPc-1** (10 µg mL^{-1}) and cet-IR700 (10 µg mL^{-1}) towards A431 cells upon NIR light irradiation in the presence of a singlet oxygen quencher, NaN$_3$ (20 mM) ($n = 4$, error bar: SD, $*p < 0.01$).

ATN-1) and non-infected control cells (MOLT-4, and TALL-1) by flow cytometry (Fig. 5b). Our findings confirmed that CD25 is highly and selectively expressed in HTLV-1-infected cells, in accordance with previous findings.[29] We therefore selected an anti-CD25 antibody, basiliximab, as a suitable antibody for NIR-PIT for the treatment of ATL.
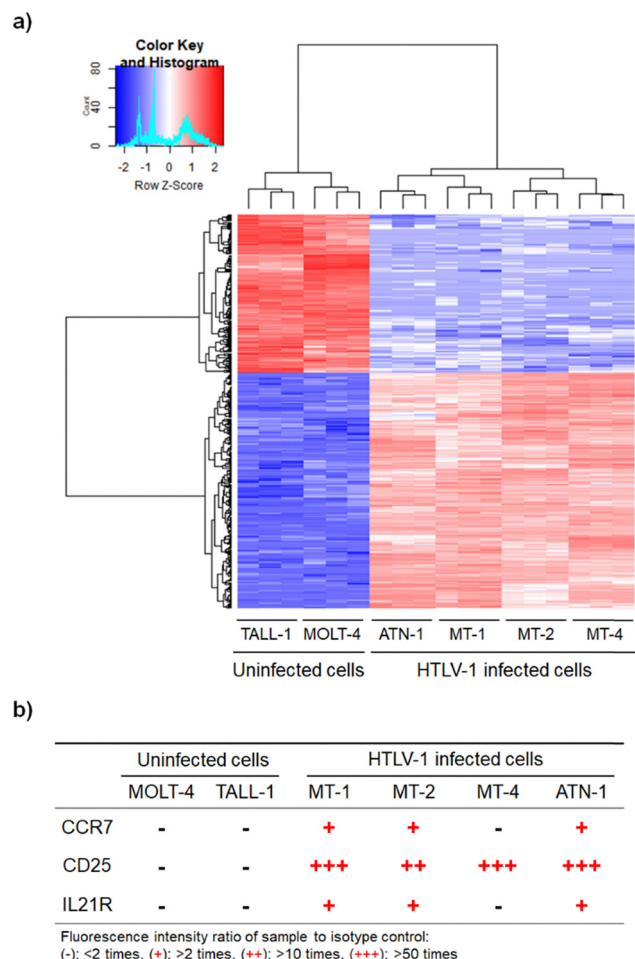
Cytotoxicity of bas-SiPc-1 against ATL

Basiliximab was labelled with **SiPc-1**, and the labelled antibody was purified by size-exclusion chromatography, then analyzed by SDS-PAGE (Fig. S5c). The drug-to-antibody ratio (DAR) of bas-**SiPc-1** was calculated to be 2.4 based on BCA assay and the absorbance spectrum (Fig. S5d). We then incubated HTLV-1-infected cells (MT-1, MT-2, MT-4, and ATN-1) and uninfected control cells (MOLT-4, and TALL-1) with bas-**SiPc-1**, irradiated them with NIR light at 690 nm, and evaluated the cytotoxicity of **SiPc-1** by WST-8 assay. Bas-**SiPc-1** selectively killed all HTLV-1-infected cell lines under photoirradiation (690 nm, 32 J cm^{-2}), while basiliximab or **SiPc-1** showed no cytotoxicity under these conditions (Fig. 6a). Further, the cytotoxicity of bas-**SiPc-1** to MT-1 cells increased in a light-dose-dependent manner. **SiPc-1** and IR700 showed similar cytotoxicity in this experiment (Fig. 6b).

Finally, we applied **SiPc-1** to clinical samples from ATL patients. Bas-**SiPc-1** was added to peripheral blood mononuclear cells (PBMC) isolated from one acute-type ATL patient (patient 1) and two chronic-type ATL patients (patients 2 and 3) (Table S1). PBMC were treated with bas-**SiPc-1** or basiliximab,

a)

b)

	Uninfected cells		HTLV-1 infected cells			
	MOLT-4	TALL-1	MT-1	MT-2	MT-4	ATN-1
CCR7	-	-	+	+	-	+
CD25	-	-	+++	++	+++	+++
IL21R	-	-	+	+	-	+

Fluorescence intensity ratio of sample to isotype control:
(-): <2 times, (+): >2 times, (++): >10 times, (+++): >50 times

Fig. 5 (a) RNA-seq analysis of HTLV-1-infected cells (MT-1, MT-2, MT-4, ATN-1) and uninfected control cells (MOLT-4, TALL-1) (n = 3). A clustering heatmap of GEP using the top 400 differentially expressed genes (DEGs). (b) Flow-cytometric analyses to examine the protein expression level of CCR7, CD25 and IL21R in HTLV-1-infected cells and uninfected control cells (n = 4).

exposed to light irradiation, and analyzed by flow cytometry within one day. The measured cell counts are shown in Table S2. In flow cytometry, the cells were firstly gated based on PBMC, followed by gating based on 7-AAD-negative live cells. The gated cells was used for further analysis (Fig. S11). PBMC from patients 1 and 2 showed high percentages of CD25+ CD4+ cells (treated with basiliximab: 79% and 75%, treated with bas-**SiPc-1**: 76% and 78%, respectively), while patient 3 showed a low percentage of CD25+ CD4+ cells (treated with basiliximab: 19%, treated with bas-**SiPc-1**: 23%) (Fig. S12a). In addition, CCR4 is a marker of HTLV-1-infected cells,[30] and patients 1 and 2 also showed high percentages of CD25+ CCR4+ cells (treated with basiliximab: 75% and 71%, treated with bas-**SiPc-1**: 73% and 69%, respectively), while patient 3 showed a low percentage (treated with basiliximab: 14%, treated with bas-**SiPc-1**: 17%) (Fig. S12b). These results suggest that patients 1 and 2 had more advanced ATL than patient 3, and confirm that CD25 can be employed as a target membrane protein for ATL.

Next, PBMC samples from the ATL patients were treated with bas-**SiPc-1** and irradiated with NIR light (690 nm, 64 or

0 J cm^{-2}), and other samples treated with non-labeled basiliximab were irradiated with NIR light (690 nm, 64 J cm^{-2}) as well. The samples were incubated at 37 °C for 24 h after the photoirradiation, then analyzed by flow cytometry. Treatment with basiliximab and light irradiation or bas-**SiPc-1** without light irradiation hardly killed CD25+ CD4+ cells (treated with basiliximab with light irradiation: patient 1:76%, patient 2:57%, patient 3:41%; treated with bas-**SiPc-1** without light irradiation: patient 1:71%, patient 2:43%, patient 3:39%). On the other hand, the tumor cell fraction (CD25+ CD4+) was specifically decreased by bas-**SiPc-1** treatment with light irradiation in patients 1, 2 and 3 (2.5%, 5.4% and 8.1%, respectively), while the other cell fractions were not decreased (Fig. 6c). We also found that the CD25+ CCR4+ fraction was selectively killed by bas-**SiPc-1** treatment with light irradiation (patient 1:1.7%, patient 2:2.8%, patient 3:1.6%, respectively), while basiliximab with light irradiation or bas-**SiPc-1** without light irradiation did not decrease the CD25+ CCR4+ fraction (treated with basiliximab with light irradiation: patient 1:73%, patient 2:54%, patient 3:36%; treated with bas-**SiPc-1** without light irradiation: patient 1:67%, patient 2:33%, patient 3:32%) (Fig. S13). These results suggest that bas-**SiPc-1** can selectively kill tumor cells derived from ATL patients.
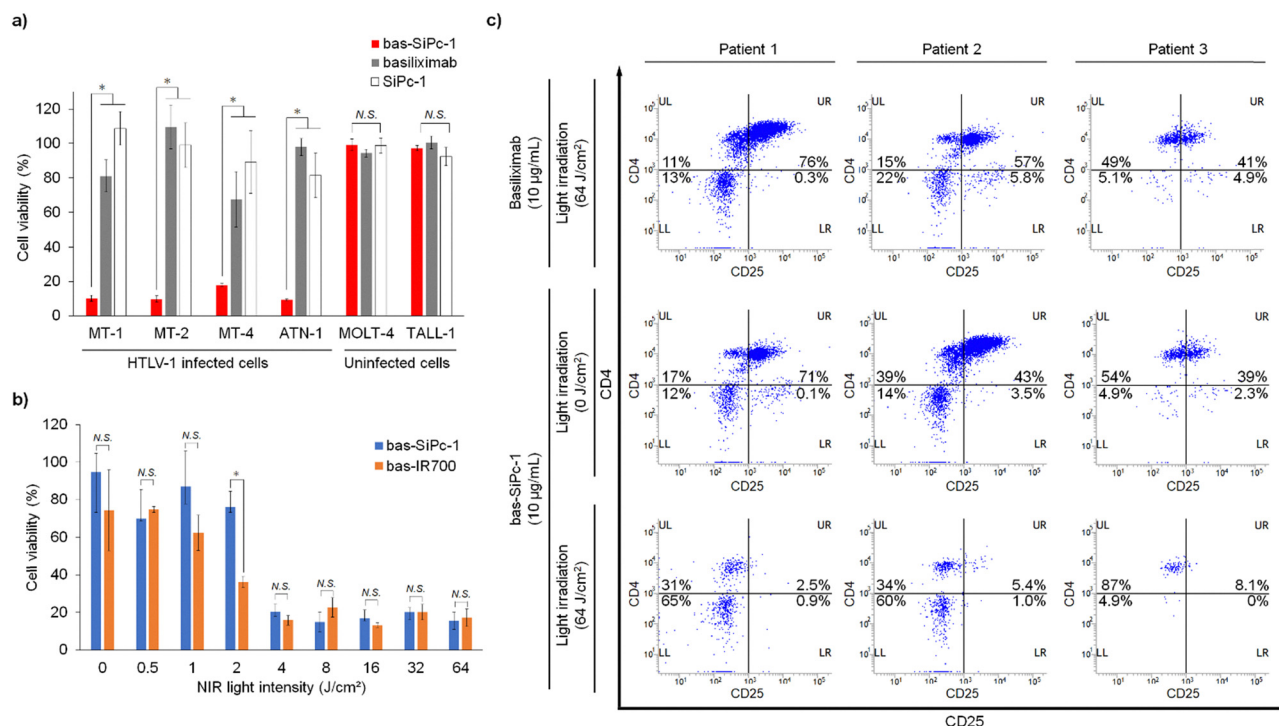
Conclusions

In conclusion, we designed **SiPc-1** by changing the linker position of IR700 from the α-position to the β-position of the phthalocyanine structure and we shortened the synthetic route by employing click chemistry to construct the linker moiety. The synthesis was completed in 8 steps. **SiPc-1** exhibits similar photophysical properties to IR700 as regards absorption and fluorescence spectra, and fluorescence and singlet oxygen production quantum yields. Although the efficacy of cleavage of the axial moieties of **SiPc-1** by photoirradiation at 690 nm was slightly lower under low-light-dose conditions compared to that of IR700, the suitability of **SiPc-1** for NIR-PIT was confirmed by the ability of cet-**SiPc-1** to induce cell damage accompanied by bleb formation in a light-dependent manner. We further applied **SiPc-1**-based NIR-PIT to tumor cells from ATL patients. Through RNA-seq gene expression analysis and protein expression level analysis by flow cytometry, CD25 was identified as a suitable target antigen for HTLV-1-infected cells. By labeling an anti-CD25 antibody with **SiPc-1**, we prepared bas-**SiPc-1**, which selectively killed tumor cells in both in culture and in human clinical samples. These results suggest that **SiPc-1** will be effective for NIR-PIT.

Furthermore, the developed synthetic procedure is expected to be available for the synthesis of a range of IR700 analogues, and thus should contribute to the further development of NIR-PIT therapy. Work along this line is currently under way. Recently, the photoimmunotherapy using compounds other than IR700 has been attempted,[31,32] and we expect that our study would also contribute to these studies.

© 2025 The Author(s). Published by the Royal Society of Chemistry

RSC Chem. Biol., 2025, **6**, 1576–1584 | 1581

Fig. 6 (a) Cytotoxicity of bas-**SiPc-1** (10 μg mL^{-1}), basiliximab (10 μg mL^{-1}) and **SiPc-1** (0.5 μM) towards HTLV-1-infected cells (MT-1, MT-2, MT-4, ATN-1) and uninfected control cells (MOLT-4, TALL-1) under NIR light irradiation (32 J cm^{-2}) at 690 nm ($n = 4$, error bar: SD, $*p < 0.01$). (b) NIR light-dependent cytotoxicity of bas-**SiPc-1** and bas-IR700 towards MT-1 cells. The cells were incubated with bas-**SiPc-1** (10 μg mL^{-1}) or bas-IR700 (10 μg mL^{-1}) at 37 °C for 1 hour. Various doses of NIR light (690 nm, 0, 0.5, 1, 2, 4, 8, 16, 32 and 64 J cm^{-2}) were applied to irradiate the cells ($n = 4$, error bar: SD, $*p < 0.01$). (c) Cytotoxicity towards the tumor cells from ATL patients treated with either basiliximab (10 μg mL^{-1}) or bas-**SiPc-1** (10 μg mL^{-1}) with or without NIR light irradiation (64 J cm^{-2}) at 690 nm. The cytotoxicity towards the CD25+ CD4+ fraction was evaluated. CD25 is the membrane protein targeted in this study, and CD4 is a marker for helper T cells transformed into ATL tumor cells. In contrast to the bas-**SiPc-1**-treated, light non-irradiated group and the basiliximab light-irradiated group, light irradiation of the bas-**SiPc-1**-treated cells selectively damaged the CD25+ CD4+ cell fraction. The percentages shown in the figure indicate the rate of cell counts within each quadrant relative to the total number of analyzed live cells.

Ethical statement

The analyses of patient samples were approved by the Institutional Review Boards of Jichi Medical University (RINS21-HEN003GO), and all subjects gave written informed consent for cryopreservation and analysis of blood samples in accordance with the Declaration of Helsinki.

Author contributions

Y. F. and K. H. planned the experiments and wrote the manuscript. Y. F. synthesized compounds, measured photophysical data, labelled dyes to antibody, RNA-seq, flow cytometry and cytotoxicity assay. M. T., S. K. and H. N. performed cytotoxicity assay with ATL clinical samples. E. S. and K. H. planned the project. H. O. advised on the synthesis. S. Y. advised on the flow cytometry measurements. M. Y., H. T., H. H. and H. K. advised on the cytotoxicity assay. All authors edited the manuscript.

Conflicts of interest

There are no conflicts to declare.

Data availability

Details of experimental methods, synthetic methods of compounds, additional spectra, HPLC trace, antibody labelling, cytotoxicity assay and fluorescence images. The data supporting this article have been included as part of the SI.

The contents of SI were composed of details of experimental methods, synthetic methods of compounds, additional spectra, HPLC trace, antibody labelling, cytotoxicity assay and fluorescence images. See DOI: **https://doi.org/10.1039/d5cb00150a**

Notes and references

1 K. Nakajima and M. Ogawa, *Int. Immunol.*, 2024, **36**, 57–64.

2 J. Kou, D. Dou and L. Yang, *Oncotarget*, 2017, **8**, 81591–81603.

3 N. Alvarez and A. Sevilla, *Int. J. Mol. Sci.*, 2024, **25**, 1023.

4 K. Sato, K. Ando, S. Okuyama, S. Moriguchi, T. Ogura, S. Totoki, H. Hanaoka, T. Nagaya, R. Kokawa, H. Takakura, M. Nishimura, Y. Hasegawa, P. L. Choyke, M. Ogawa and H. Kobayashi, *ACS Cent. Sci.*, 2018, **4**, 1559–1569.

5 M. Mitsunaga, M. Ogawa, N. Kosaka, L. T. Rosenblum, P. L. Choyke and H. Kobayashi, *Nat. Med.*, 2011, **17**, 1685–1691.

6 T. Moriya, M. Hashimoto, H. Matsushita, S. Masuyama, R. Yoshida, R. Okada, A. Furusawa, D. Fujimura, H. Wakiyama, T. Kato, P. L. Choyke, Y. Kusumoto, T. Chtanova, H. Kobayashi and M. Tomura, *Cancer Immunol., Immunother.*, 2022, **71**, 3099–3106.

7 M. Ogawa, Y. Tomita, Y. Nakamura, M.-J. Lee, S. Lee, S. Tomita, T. Nagaya, K. Sato, T. Yamauchi, H. Iwai, A. Kumar, T. Haystead, H. Shroff, P. L. Choyke, J. B. Trepel and H. Kobayashi, *Oncotarget*, 2017, **8**, 10425–10436.

8 T. Nagaya, J. Friedman, Y. Maruoka, F. Ogata, S. Okuyama, P. E. Clavijo, P. L. Choyke, C. Allen and H. Kobayashi, *Cancer Immunol. Res.*, 2019, **7**, 401–413.

9 M. Tahara, S. Okano, T. Enokida, Y. Ueda, T. Fujisawa, T. Shinozaki, T. Tomioka, W. Okano, M. A. Biel, K. Ishida and R. Hayashi, *Int. J. Clin. Oncol.*, 2021, **26**, 1812–1821.

10 D. M. Cognetti, J. M. Johnson, J. M. Curry, S. T. Kochuparambil, D. McDonald, F. Mott, M. J. Fidler, K. Stenson, N. R. Vasan, M. A. Razaq, J. Campana, P. Ha, G. Mann, K. Ishida, M. Garcia-Guzman, M. Biel and A. M. Gillenwater, *Head Neck*, 2021, **43**, 3875–3887.

11 T. Kato, R. Okada, Y. Goto, A. Furusawa, F. Inagaki, H. Wakiyama, H. Furumoto, D. Daar, B. Turkbey, P. L. Choyke, H. Takakura, O. Inanami, M. Ogawa and H. Kobayashi, *ACS Pharmacol. Transl. Sci.*, 2021, **4**, 1689–1701.

12 H. Furumoto, R. Okada, T. Kato, H. Wakiyama, F. Inagaki, H. Fukushima, S. Okuyama, A. Furusawa, P. L. Choyke and H. Kobayashi, *Cancers*, 2022, **14**, 4042.

13 X. Peng, D. R. Draney and J. Chen, *PHTHALOCYANINE DYES*, WO 2004/038378A2, World Intellectual Property Organization, 2004.

14 K. Takahashi, A. Sugiyama, K. Ohkubo, T. Tatsumi, T. Kodama, K. Yamatsugu and M. Kanai, *Synlett*, 2021, 1098–1103.

15 M. Kobayashi, M. Harada, H. Takakura, K. Ando, Y. Goto, T. Tsuneda, M. Ogawa and T. Taketsugu, *ChemPlusChem*, 2020, **85**, 1959–1963.

16 E. D. Anderson, A. P. Gorka and M. J. Schnermann, *Nat. Commun.*, 2016, **7**, 13378.

17 H. Takakura, Y. Goto, A. Kitamura, T. Yoshihara, S. Tobita, M. Kinjo and M. Ogawa, *J. Photochem. Photobiol., A*, 2021, **408**, 113094.

18 O. Inanami, W. Hiraoka, Y. Goto, H. Takakura and M. Ogawa, *ChemPhotoChem*, 2022, **6**, e202100172.

19 D. Kamakura, R. Asano, H. Kawai and M. Yasunaga, *Cancer Immunol. Immunother.*, 2021, **70**, 177–188.

20 H. Katsuya, K. Ishitsuka, A. Utsunomiya, S. Hanada, T. Eto, Y. Moriuchi, Y. Saburi, M. Miyahara, E. Sueoka, N. Uike, S. Yoshida, K. Yamashita, K. Tsukasaki, H. Suzushima, Y. Ohno, H. Matsuoka, T. Jo, M. Amano, R. Hino, M. Shimokawa, K. Kawai, J. Suzumiya and K. Tamura, *Blood*, 2015, **126**, 2570–2577.

21 G. Forlani, M. Shallak, R. S. Accolla and M. G. Romanelli, *Int. J. Mol. Sci.*, 2021, **22**, 8001.

22 A. Lavorgna and E. W. Harhaj, *Viruses*, 2014, **6**, 3925–3943.

23 M. Mahgoub, J. I. Yasunaga, S. Iwami, S. Nakaoka, Y. Koizumi, K. Shimura and M. Matsuoka, *Proc. Natl. Acad. Sci. U. S. A.*, 2018, **115**, E1269–E1278.

24 Y. Imaizumi, M. Iwanaga, K. Nosaka, K. Ishitsuka, K. Ishizawa, S. Ito, M. Amano, T. Ishida, N. Uike, A. Utsunomiya, K. Ohshima, J. Tanaka, Y. Tokura, K. Tobinai, T. Watanabe, K. Uchimaru, K. Tsukasaki, A. Takaori, M. Hishizawa, A. Kitanaka, A. Takami, A. Ito, K. Yonekura, A. Mugitani, C. Kato, D. Ogawa, D. Tsuruta, E. Ohtsuka, Y. Saburi, E. Sueoka, F. Kazuyasu, M. Yoshimitsu, F. Matsubara, F. Miyagawa, F. Nakamura, M. Sugaya, H. Kobayashi, H. Heizan, H. Fuse, H. Shibayama, H. Yamaguchi, H. Ishikawa, S. Yoshida, H. Iwasaki, H. Kawano, H. Kazama, H. Yamasaki, H. Kuroda, M. Yamada, H. Suzushima, I. Choi, N. Uike, K. Miyashita, K. Saigo, K. Ohshiro, K. Tatsuno, T. Ono, K. Sugimoto, K. Ohmachi, K. Etoh, M. Koga, K. Narukawa, K. R. Koh, K. Uozumi, K. Nagai, K. Adachi, T. Motokura, K. Izutsu, K. Kato, K. Nagafuji, M. Yuge, M. Miyahara, M. Higuchi, M. Hayashi, M. Iino, M. Makita, M. Hagihara, M. Shibano, M. Ito, M. Saito, M. Koike, M. Hidaka, M. Kurosawa, M. Fukazawa, M. Shindo, M. Takenaka, N. Kobayashi, N. Kosugi, N. Nakamura, N. Tominaga, N. Fukuhara, R. Sakai, R. Nawata, S. Iyama, S. Yamasaki, S. Nakachi, T. Tomoyose, S. Chiba, S. Rai, T. Okada, T. Shimano, T. Inozume, T. Ito, T. Ikezoe, T. Fujimoto, T. Jo, T. Kaji, T. Murayama, T. Myojo, T. Takahashi, T. Takahashi, T. Yujiri, T. Nakayama, Y. Adachi, Y. Kato, Y. Kobayashi, Y. Moriuchi, Y. Ogata and Y. Katayama, *Cancer Sci.*, 2020, **111**, 4567–4580.

25 Y. Inoue, S. Fuji, R. Tanosaki, Y. Inamoto, T. Tanaka, A. Ito, K. Okinaka, S. Kurosawa, S. W. Kim, H. Nakagama and T. Fukuda, *Bone Marrow Transplant.*, 2018, **53**, 1105–1115.

26 A. Utsunomiya, I. Choi, D. Chihara and M. Seto, *Cancer Sci.*, 2015, **106**, 344–351.

27 A. Utsunomiya, *Front. Microbiol.*, 2019, **10**, 2235.

28 G. P. Taylor and L. B. Cook, *Br. J. Haematol.*, 2022, **198**, 941–942.

© 2025 The Author(s). Published by the Royal Society of Chemistry

RSC Chem. Biol., 2025, **6**, 1576–1584 | 1583

29 K. Karube, K. Ohshima, T. Tsuchiya, T. Yamaguchi, R. Kawano, J. Suzumiya, A. Utsunomiya, M. Harada and M. Kikuchi, *Br. J. Haematol.*, 2004, **126**, 81–84.

30 K. Kataoka, Y. Nagata, A. Kitanaka, Y. Shiraishi, T. Shimamura, J. I. Yasunaga, Y. Totoki, K. Chiba, A. Sato-Otsubo, G. Nagae, R. Ishii, S. Muto, S. Kotani, Y. Watatani, J. Takeda, M. Sanada, H. Tanaka, H. Suzuki, Y. Sato, Y. Shiozawa, T. Yoshizato, K. Yoshida, H. Makishima, M. Iwanaga, G. Ma, K. Nosaka, M. Hishizawa, H. Itonaga, Y. Imaizumi, W. Munakata, H. Ogasawara, T. Sato, K. Sasai, K. Muramoto, M. Penova, T. Kawaguchi, H. Nakamura, N. Hama, K. Shide, Y. Kubuki, T. Hidaka, T. Kameda, T. Nakamaki, K. Ishiyama, S. Miyawaki, S. S. Yoon, K. Tobinai, Y. Miyazaki, A. Takaori-Kondo, F. Matsuda, K. Takeuchi, O. Nureki, H. Aburatani, T. Watanabe, T. Shibata, M. Matsuoka, S. Miyano, K. Shimoda and S. Ogawa, *Nat. Genet.*, 2015, **47**, 1304–1315.

31 L. Tu, C. Li, Q. Ding, A. Sharma, M. Li, J. Li, J. S. Kim and Y. Sun, *J. Am. Chem. Soc.*, 2024, **146**, 8991–9003.

32 C. Li, L. Tu, Y. Xu, M. Li, J. Du, P. J. Stang, Y. Sun and Y. Sun, *Angew. Chem., Int. Ed.*, 2024, **63**, e202406392.